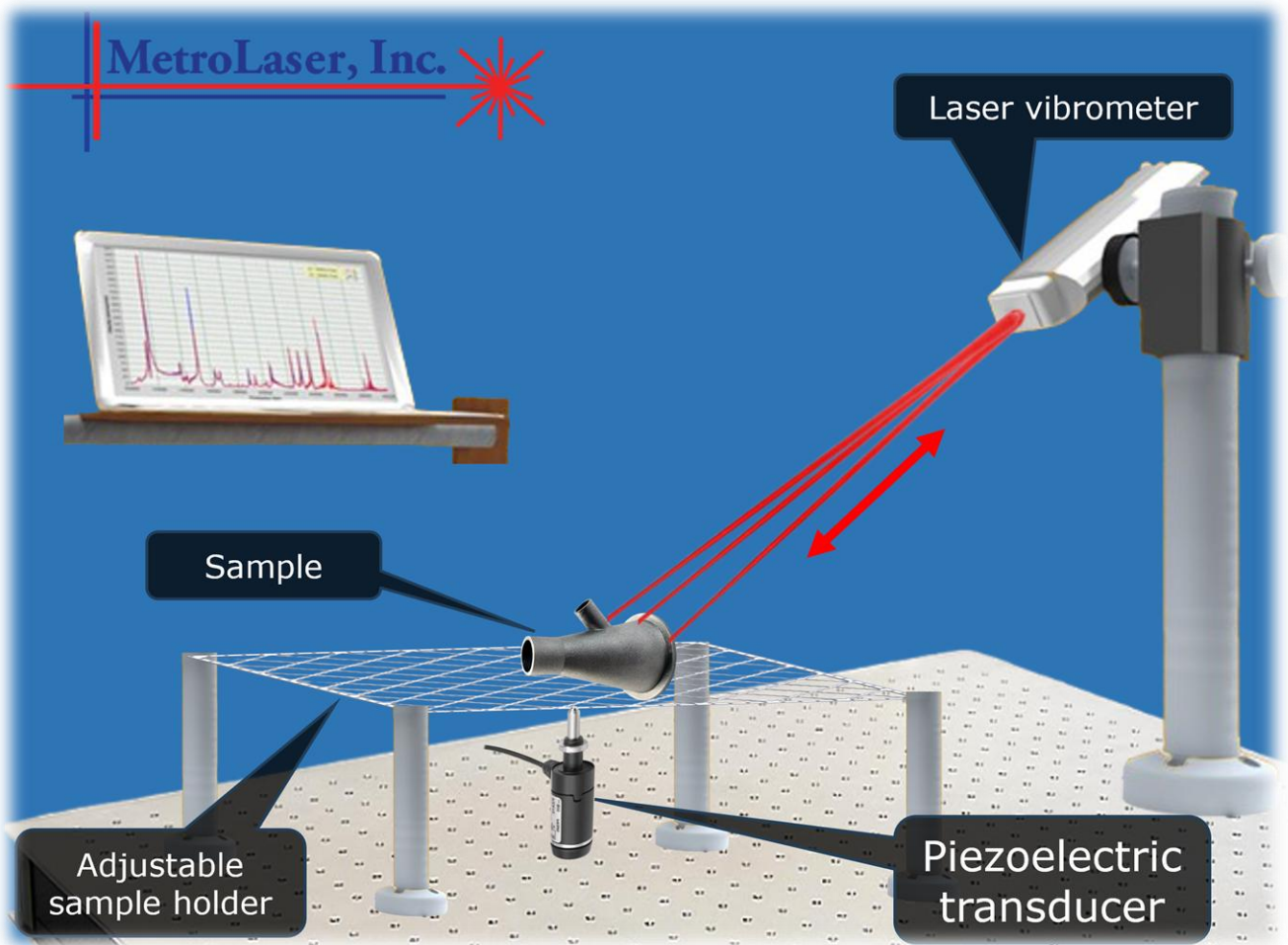


Laser Acoustic Resonance Spectroscopy (LARS)

Application Notes



- Non-destructive evaluation
- Minimal sample preparation
- Digital rendering of vibrational modes
- Computational modeling

- Wide range of applicable materials
- High confidence
- Rapid testing
- Immediate evaluation

Background

LARS is primarily used for detection of defects in metallic parts. One type of defect that is detectable by LARS but not by typical inspection methods is an internal void in an additively manufactured part. In this application note, we demonstrate detection of such a void, as well location of that void, using LARS.

Brackets

Additively manufactured AlSi10Mg brackets with intentional voids were manufactured and tested with LARS. These brackets were 6.5" and 3" in the long and short sides, 2" wide, and 0.125" thick. We tested 22 brackets in total, with 4 built with no programmed defects, and 18 with programmed defects as follows:

1. Four parts (L1-L4) with no programmed defects
2. Three parts (M1-M3) with a large defect in the bottom location
3. Three parts (M4-M6) with a large defect in the middle location
4. Three parts (N1-N3) with a mid-size defect in the bottom location
5. Three parts (N4-N6) with a mid-size defect in the middle location
6. Three parts (O1-O3) with a small defect in the bottom location
7. Three parts (O4-O6) with a small defect in the middle location

The defects (voids) were programmed with a thickness of 0.045", leaving a wall of 0.040" on each side of the defect. The lateral dimensions of the defects were 1.2" x 0.6" (large), 0.6" x 0.6" (medium), and 0.6" x 0.3" (small). Drawings of the parts are shown below in **Figure AN 1.1**.

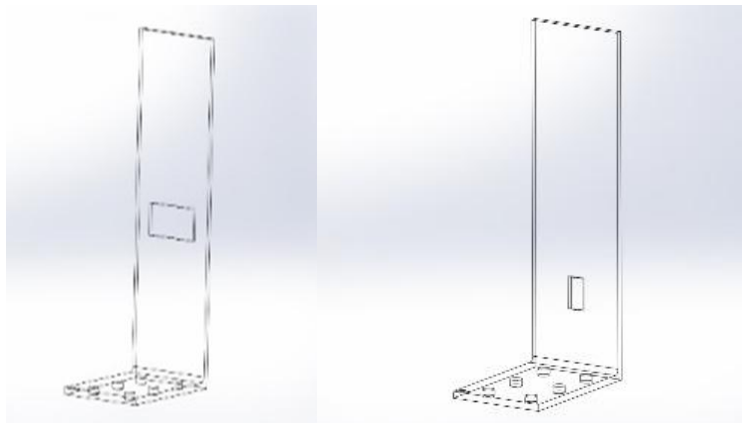


Figure AN 1.1. Cross section of the brackets showing a manufactured defect in the (a) bottom section, and (b) middle section.

Application Note 1

Detection of Voids in Brackets

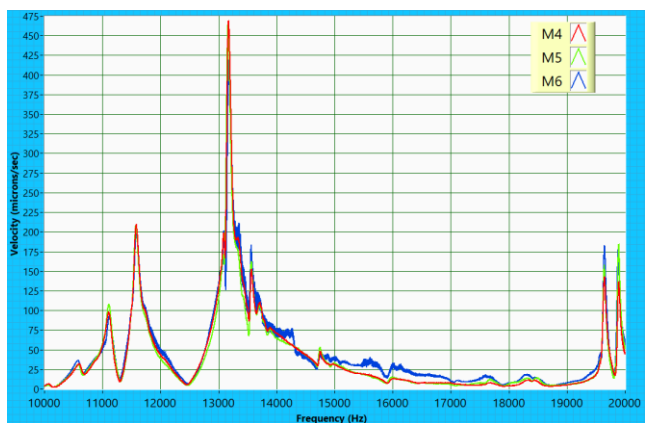


Figure AN 1.2. The spectra for three parts with a large defect in the center, M4-M6.

LARS Spectra

The spectra within a group were consistent, as shown in **Figure AN 1.2**. An extremely obvious difference exists between the defect free L1 and M1, with a large defect, as shown in **Figure AN 1.3**. The difference between the defect free bracket and the bracket with a small defect (O1) is smaller but still present in **Figure AN 1.4**.

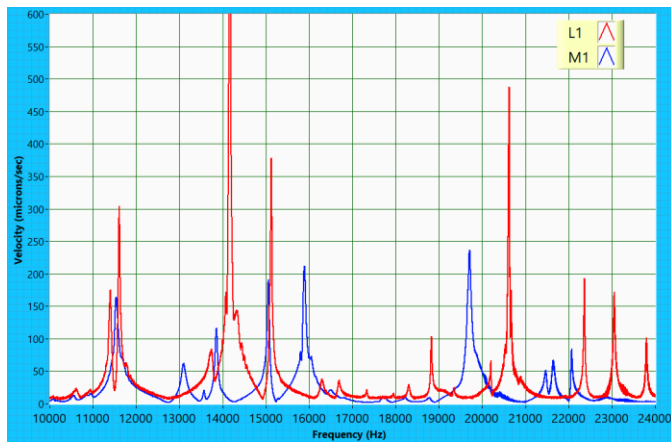


Figure AN 1.3. Measured vibration spectra of L1 (defect free) and M1 (large defect) between 16-24 kHz, illustrating distinct differences in the spectra.

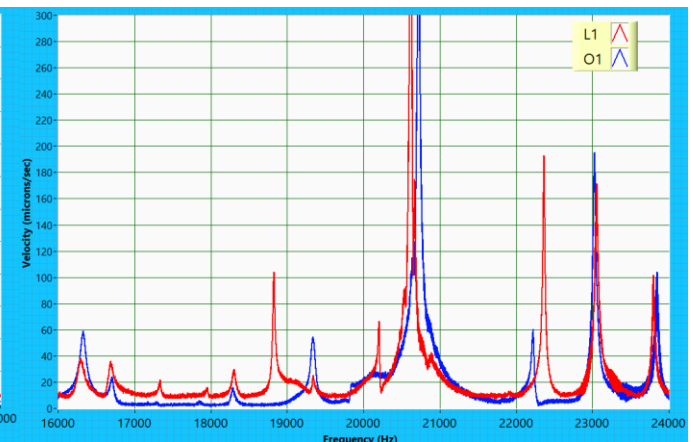


Figure AN 1.4. The measured spectra for L1 (defect free) and O1 (smallest defect) between 16-24 kHz, illustrating clear differences in the spectra.

Vibrational Mode Shapes

LARS is not only capable of measuring vibrational spectra, but also the shapes of resonance modes. This can be useful for defect localization, as demonstrated here, as well as validating FE models, since predicted resonance modes can be compared in both frequency and shape to measurements.

Figures AN 1.5 - AN 1.8 show this for the brackets. The amplitude of resonance modes are larger above the defect, and the shape is clearly affected by a defect's presence. Additionally, the shift in frequency of about 100 Hz can be seen between **Figure AN 1.5** and **Figure AN 1.6**.

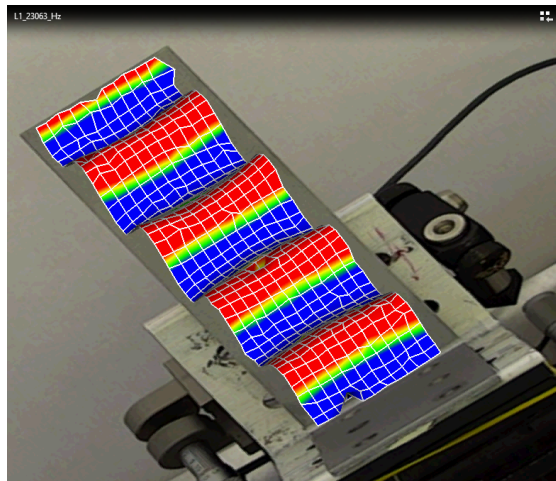


Figure AN 1.5. Measured vibration mode at 23,063 Hz for L1 (defect free).

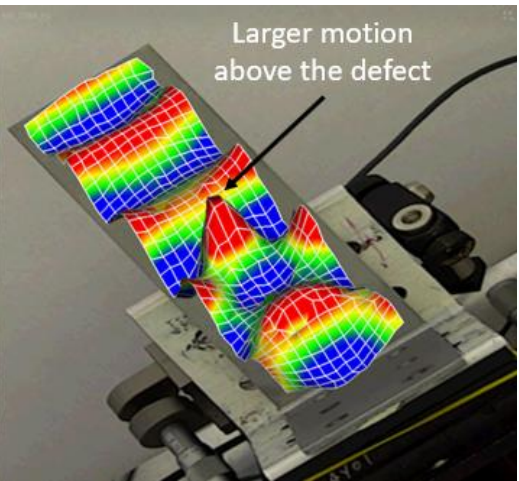


Figure AN 1.6. Measured vibration mode at 22,964 Hz for M5 (large defect, middle region).

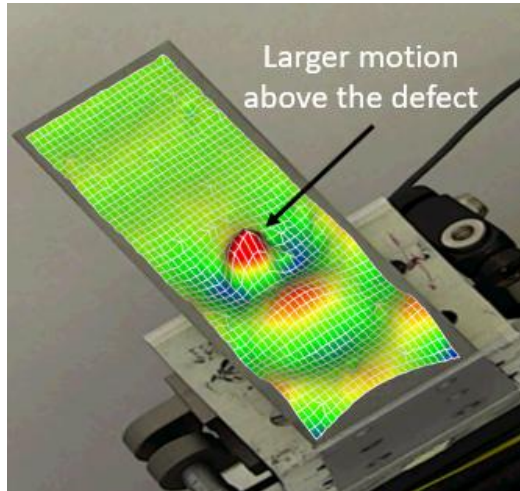


Figure AN 1.7. Measured vibration mode at 28,472 Hz for N4 (medium defect, middle region).

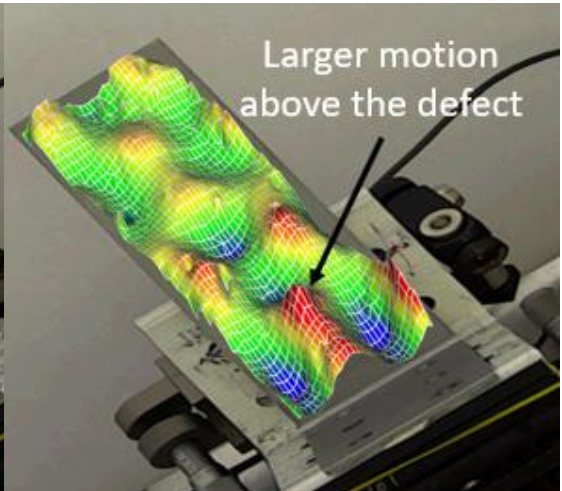


Figure AN 1.8. Measured vibration mode at 38,034 Hz for O1 (small defect, bottom region).

Part Clustering

Sometimes, no known good reference part is available. Instead, it is expected that most parts are good and only a few parts deviate from that good group. Additionally, one may want to identify parts with similar defects to each other. In this case, a strategy using machine learning based clustering analysis is effective.

As an example, clustering analysis was run on the L1-3, M1-6, N1-6, O1, O2, O4, L2_2 (repeat measurement of L2), Y7 (pristine bracket printed in a later print run) and Y5 (pristine bracket with a different print orientation, leading to significantly different elastic properties but the same geometry). The input to this clustering process is exclusively the measured spectra; no information about how the parts are truly related is given to the clusterer (Agglomerative Clustering or HBDSCAN).

Agglomerative clustering requires the user to define the number of clusters; here, 8 clusters were used.

A dendrogram for the Agglomerative Clustering results is shown in **Figure AN 1.9**. A very similar dendrogram is produced by HBDSCAN, which does not have a pre-defined number of clusters. The only difference in HBDSCAN results is that the small and medium defects at location B (O4 and N4-N6) are combined into a single group.

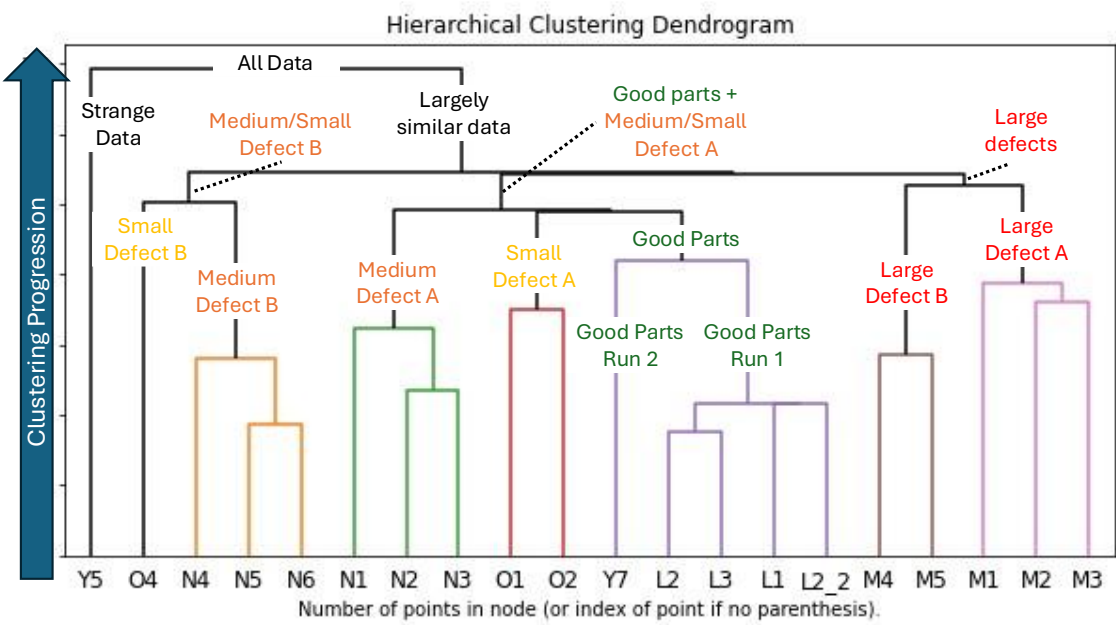


Figure AN 1.9. Hierarchical Clustering Dendrogram for Agglomerative Clustering of intentionally defective brackets with labels added post-processing.

Part Clustering Success

One notices that agglomerative clustering not only produces a precisely correct result but also groups the brackets into intuitive groups and subgroups. The clustering program runs from bottom to top in **Figure AN 1.9**, but it is easier to explain intuitively from top to bottom. Starting with all of the data, the strange data from Y5, which has different elastic properties than the rest, is split off first. Then, the rest of the data is split between super-clusters of large defects, medium and small defects at location B, and the rest of the parts. The three super-clusters then split into groups that match exactly the known groups, forming separate clusters for good parts and each different defect size and location.

Again, these clusters formed with no information except for LARS spectra. This result shows the power of LARS spectra for identifying defects and even separating parts with similar types of defects. While this technique does not directly validate parts, it can be used in combination with other strategies or be used to separate small populations of defective parts from much larger populations of good parts.

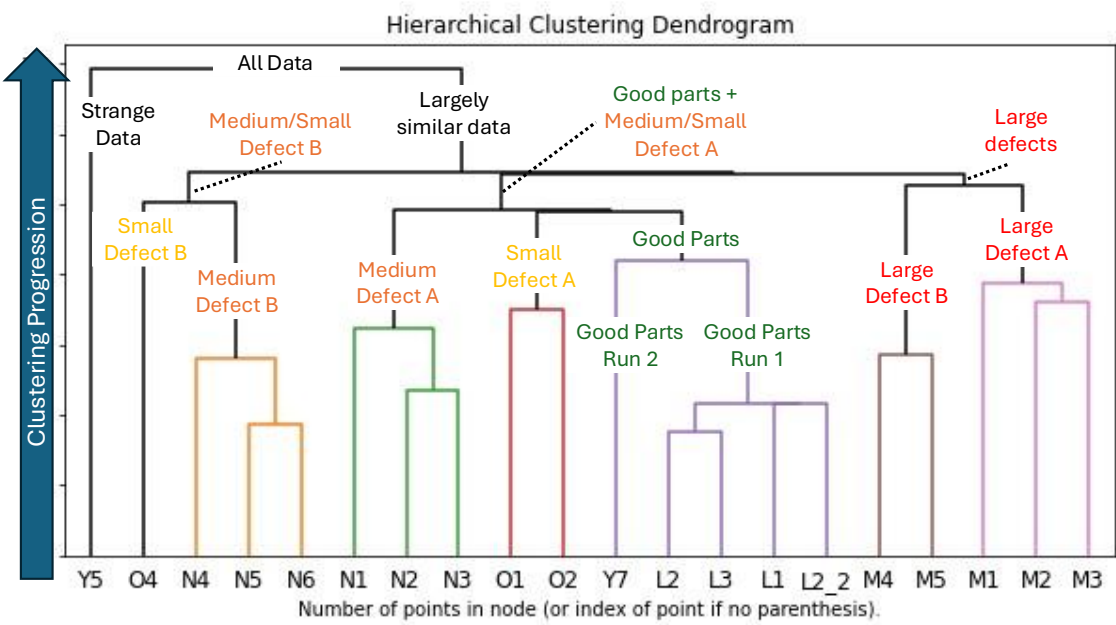


Figure AN 1.9. Hierarchical Clustering Dendrogram for Agglomerative Clustering of intentionally defective brackets with labels added post-processing.

Machine Learning Classification

Other times, one or more known good reference parts exist, or the resonance spectrum of a good part can be confidently calculated from a CAD model. Then, part classification as good or bad is a matter of comparison to that reference spectrum. We have developed a proprietary machine learning based classification algorithm to speed up and simplify this comparison so that LARS is accessible and useful without expertise in vibrational mechanics. This algorithm's output is a score from 0 to 1, indicating the similarity to the known good part.

Using the bracket data, L1 was used as a reference part. Then, parts' similarity was scored, with the results shown in **Figure AN 1.10**. Like the clustering algorithms in the previous section, the machine learning classification algorithm is not given any information about the true known defects in the brackets. Nonetheless, the small, medium, and large defects are clearly identified and separated from the good parts (L3, L4, and Y7).

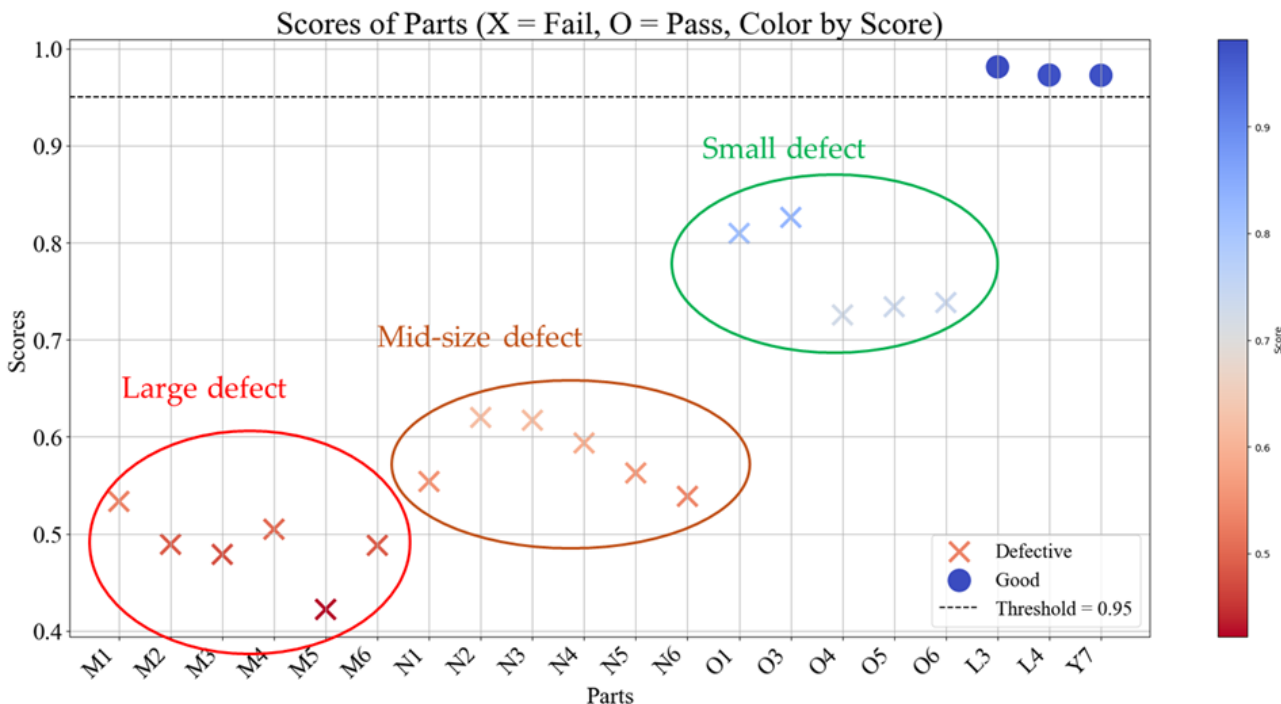


Figure AN 1.10. Classification of defective brackets using the proposed ML method.

Background

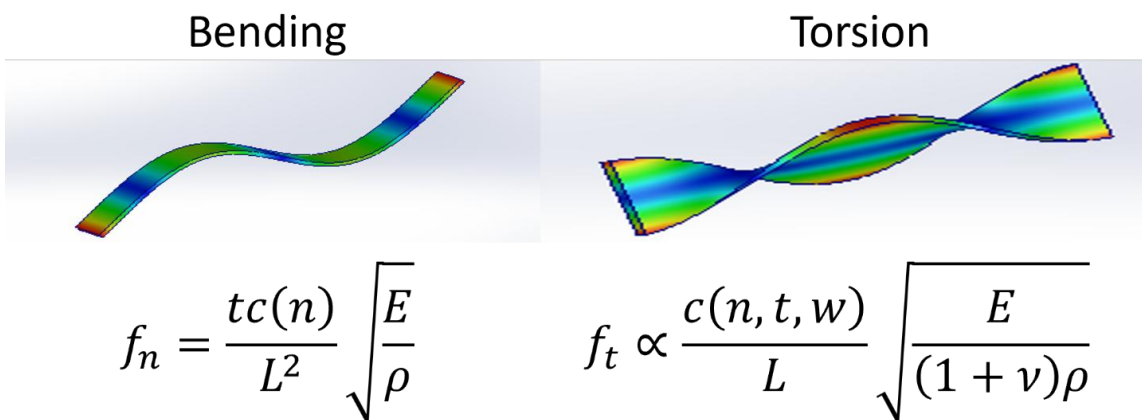
LARS can be used to validate FE models by simultaneously confirming or detecting differences in the dimensions and elastic properties of the object. The resonant frequencies of different vibrational modes of a part are dependent on the dimensions, modulus, and Poisson's ratio of a part in different ways. Therefore, changes in dimensions or elastic properties which both cause resonance frequencies to shift can be disambiguated.

LARS can be used to measure elastic properties of a sample nondestructively and more accurately than a standard tensile test. Rectangular bars provide a clear example of this and are studied in this application note.

Samples – Steel Bars of various alloys

We studied two samples each of 1/8" x 1" x 12" bars of four different steel alloys: 303 stainless steel (303SS), 4140 steel, A2 steel, and low carbon steel (LCS). These are all expected to have moduli and Poisson's ratios within ~10% of each other.

For rectangular bars, there are two prominent modes measured easily by LARS – bending and torsion modes as shown in Figure AN 2.1. The figure also shows how the resonance frequencies of the n^{th} mode f_n vary differently with the modulus and Poisson's ratio of the bars, as well as the geometry.



E – Young's Modulus, ρ – Density, ν – Poisson's ratio
 L – length, w – width, t – thickness, c – const. function

Figure AN 2.1. For a bar (and any other geometry), peaks associated with different mode shapes shift differently due to changes of dimensions and elastic properties.

LARS Spectra

The bars used in our experiment were precisely cut to their dimensions, so the modulus and Poisson's ratio differences between the alloys are expected to completely dominate any dimensional effect on the resonance frequencies. The difference was apparent between all of the alloys; below is an example with LCS and 303SS. The raw LCS spectrum measured by LARS is plotted in **Figure AN 2.2** in blue.

The raw spectrum for 303SS does not match up with the LCS spectrum, as expected due to elastic differences. Instead, we "stretch" the 303SS spectrum by multiplying the frequencies by a constant. The 303SS spectrum is stretched by 6.3% (i.e., frequencies multiplied by 1.063) to arrive at the green spectrum plotted in the figure. With that stretching, many but not all of the peaks match the blue LCS data. Most of the remaining peaks are matched if the 303SS spectrum is instead stretched by 3.7%.

From **Figure AN 2.1**, it is expected that one of these stretching values corresponds to bending modes and the other to torsion modes. The peaks labeled gray in **Figure AN 2.2** don't match after either stretching and are possibly a complicated mode that combines both. LARS offers the ability to confirm this analysis in detail by measuring the mode shapes at the desired frequencies. The insets show a torsion mode (5.07 kHz) and bending mode (5.63 kHz) corresponding to peaks labeled orange and green, respectively (i.e., associated with a 6.3% and 3.7% difference in frequency).

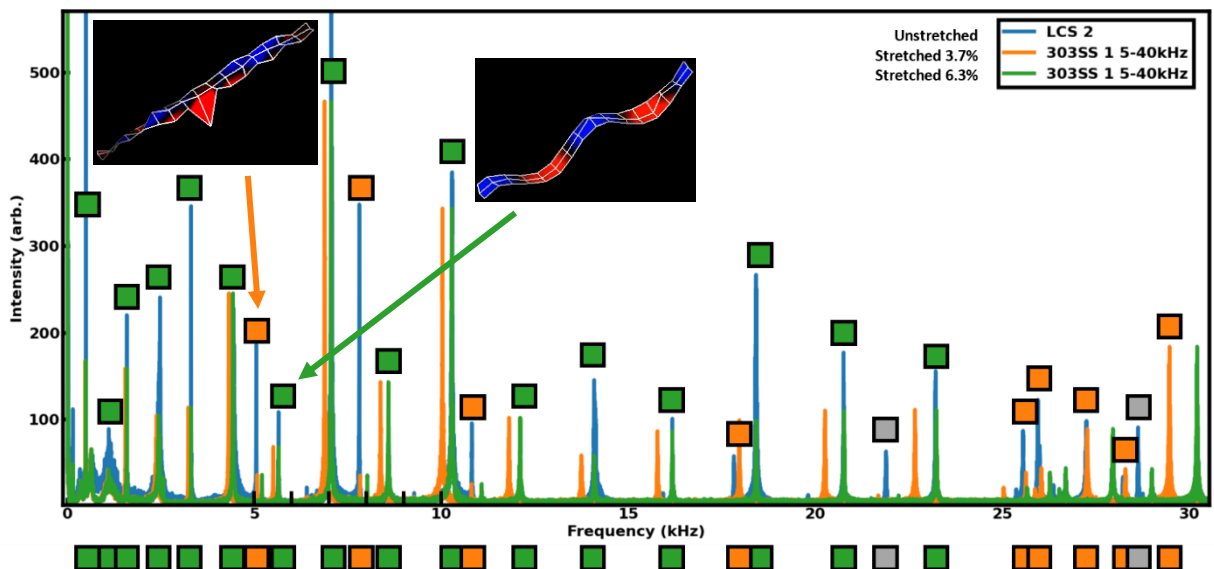


Figure AN 2.2. LCS differed from 303SS in bending (green) by a scaling factor 6.3% and torsion (orange) by 3.7%.

Quantitative Analysis

The resonance frequencies for a 303SS bar with a modulus $E = 190 \text{ GPa}$, density $\rho = 8 \text{ g/cc}$, and Poisson's ratio $\nu = 0.25$ were calculated and compared to the measured frequencies. These were separated into bending and torsion modes so that the equations in **Figure AN 2.1** can be used to calculate the true mechanical properties of the measured bar. **Figure AN 2.3** shows the measurement compared to the FEA calculations as well as the residuals of fit lines for the torsion and bending mode frequencies.

The excellent correlation between the theory and measurement, as well as the small and randomly distributed residuals for the bending modes confirm that the theory is representative of the real behavior of the part. That the torsion residuals are small but not distributed randomly suggests a minor dimensional difference between the FEA model and the part, since changes in the thickness or width cause nonlinear changes in torsion mode frequencies.

Ignoring these small dimensional errors, from the slopes of the fit lines, we can calculate the true E/ρ ratio and the true ν . These are $E/\rho = 25.74 \text{ mm}^2/\mu\text{s}^2$ (rather than the theory $23.75 \text{ mm}^2/\mu\text{s}^2$) and 0.275 . Assuming the density was correct, this corresponds to a true E of 206 GPa .

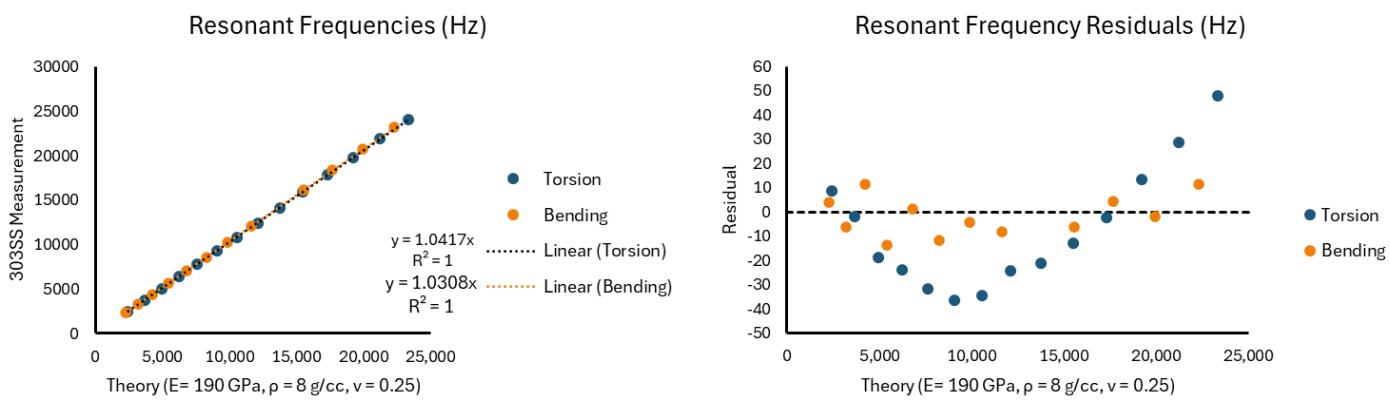


Figure AN 2.3. Measured resonant frequencies in bending and torsion compared to FEA-calculated values, and fit residuals for the line fit.

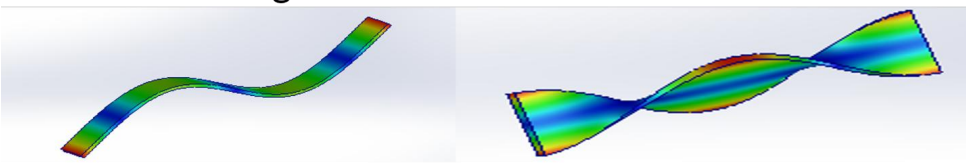
Conclusion

Using LARS, we were able to precisely determine absolute and relative values of the elastic properties for steel bars of various alloys. We saw that measurement of multiple different mode shapes enabled the determination of multiple parameters (Young’s modulus and Poisson’s ratio). This allowed a FE model to be updated with the appropriate properties and predict the resonant frequencies of the sample well.

LARS is an effective and nondestructive tool for validating FE models by measuring true vibrational responses and comparing them to those calculated from the FE model. An FE model can be iteratively updated (in the case of simple geometries like a bar, with help from analytical formulae) to match the true resonances, revealing differences in dimensions and elastic properties.

Bending

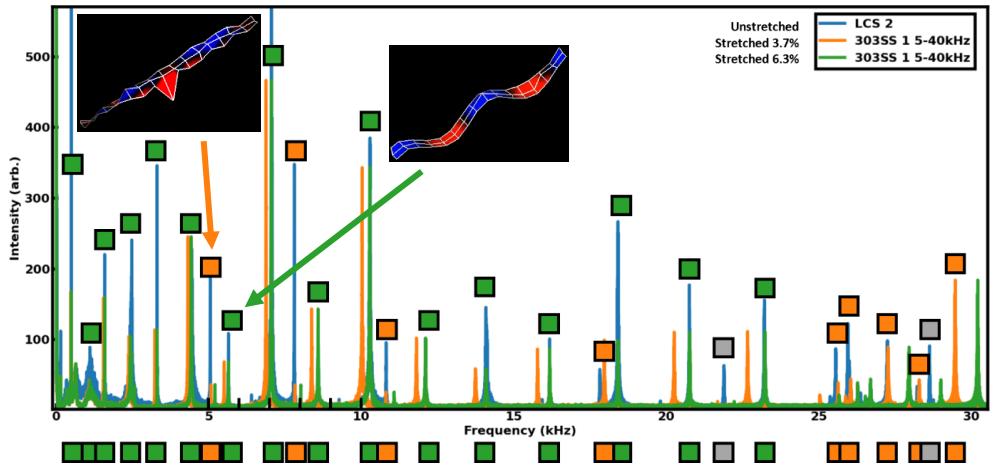
Torsion



$$f_n = \frac{tc(n)}{L^2} \sqrt{\frac{E}{\rho}}$$

$$f_t \propto \frac{c(n, t, w)}{L} \sqrt{\frac{E}{(1 + \nu)\rho}}$$

E – Young’s Modulus, ρ – Density, ν – Poisson’s ratio
 L – length, w – width, t – thickness, c – const. function



Laser Acoustic Resonance Spectroscopy (LARS)

Available upon inquiry:

Instrument for direct purchase

Technical services:

Nondestructive quality assurance, authentication, and vibrational characterization

MetroLaser Inc.
22941 Mill Creek Drive
Laguna Hills, CA 92653, USA
Ph: (949) 553-0688 ext. 244
Fax: (949) 553-0495
Email: sales@metrolaserinc.com

